Available online at www.sciencedirect.com

jmr&t Journal of Materials Research and Technology

https://www.journals.elsevier.com/journal-of-materials-research-and-technology

Original Article

The evolution of the microstructure and properties of ageable Al-Si-Zn-Mg alloy during the recycling of milling chips through powder metallurgy

*P.A. Pulido-Suárez, K.S. Uñate-González, J.G. Tirado-González, A. Esguerra-Arce, J. Esguerra-Arce**

CIMSER, Industrial Engineering Department, Escuela Colombiana de Ingeniería Julio Garavito, AK.45 No. 205-59 (Autopista Norte), Bogotá, Colombia

ARTICLE INFO

Article history:
Received 7 May 2020
Accepted 11 August 2020
Available online 28 August 2020

Keywords:
Composite
Discontinuous chips
Powder metallurgy
Aluminum alloys
Dynamic recrystallization

ABSTRACT

Although long/continuous metallic chips are easily recycled by melting, this is not the case for discontinuous milling chips. The present study aimed to reduce waste generation and to facilitate the use of this byproduct in order to obtain a metallic-oxide composite. Chips were collected after machining Al-Si-Zn-Mg alloy parts, and powders were obtained through grinding processes. Grinding was performed at 45, 69, and 94 h, with grinding bodies/chips volume ratios of 6:1, 8:1, 10:1 and 12:1. The resulting powders were characterized by scanning electron microscopy, laser granulometry, and X-ray diffraction. After grinding, the particles were compacted and sintered, and hardness was evaluated. It was found that metallic powder is formed through plastic deformation, hardening, fracture, and dynamic recrystallization. It was possible to obtain samples with lower apparent density and higher hardness by powder metallurgy from Al-Si-Zn-Mg alloy chips than from the bulk. Powder was obtained after grinding, and samples were obtained by compacting and sintering. The higher hardness value was attributed to the presence of Al_2O_3 formed in the particles during grinding, which acts as a second reinforcing phase in the sintered samples, and as a retardant of intermetallic phase growing.

1. Introduction

Aluminum alloys are used in the automotive [1], aeronautic—aircraft fuselages, wings, engines, etc.—[2], and other industries as well in the military [3], due to their properties of high strength to weight ratio, and high corrosion and fatigue resistance. These are processed from, among other manufacturing methods, material removal through machining, which is a manufacturing technique that consists of removing material from a solid piece to obtain a piece of a required geometry. These processes include drilling, turning and milling. The removed material remains in the form of chips. Statistics are lacking on the amount of metal that becomes chips during machining, but it has been estimated that 25% of aluminum scrap is in the form of chips [4].

* *Corresponding author.*
E-mail: johanna.esguerra@escuelaing.edu.co (J. Esguerra-Arce).

https://doi.org/10.1016/j.jmrt.2020.08.045

The typical way to recycle metal residues is by melting. However, in the case of machining chips produced by drilling, turning and milling, the process of recycling by melting is more difficult. The difficulties with this are related to the low bulk density and high surface area, which produces a lot of oxide in the surface of the scrap. This oxide mixes with the slag and is lost. It has been estimated that the average metal loss in the melting of long and helical chips is about 20%, as reported by Gronostajski et al. [5]. Taking into account the entire process the quantified losses are even greater:

- Part of the metal is burnt, which results in losses of 10%
- Part of the metal mixes with the slag and is removed from the surface. This is made worse because of the low density of the melted aluminum, which causes it to stay for a relatively long time on the surface and to oxidize intensively. This results in losses of 10%.
- During the ingot process, there are losses of about 18%.

Later, Gronostajski et al. [6] conclude that no more than 54% of the metal is recovered, when the material is in form of helical chips. In the case of discontinuous and short chips, the picture is worse, because this kind of chip exhibits a greater surface area than long and helical chips.

Another option is to recycle them by means of compaction and sintering, but the obtained hardness is very low in comparison to the original material [7]. Meanwhile, powder metallurgy has been successfully applied to reuse aluminum scrap by producing pieces from metal powder. This includes re-melting to obtain powders by the centrifugal atomization process, with hardness about 60 Rockwell F [8], and by the production of metal powder by ball grinding processes [9–11]. Fuziana et al. [10], ground 6061 alloy chips, finding that the green density of compacted samples depends on the rotational speed of the ball mill, and that it is possible to obtain sintered samples up to 100 Rockwell F hardness. Rojas-Díaz et al. [11], who ground commercially pure aluminum chips, found that the morphology and size distribution of the produced Al powder depend strongly on the grinding time. Moreover, they found that it is possible to obtain sintered pieces with this powder with more than 95% of the original hardness of 90.6 Rockwell F.

However, there are no studies on the effect of grinding time and grinding bodies/chips volume ratio on the hardness of samples of sintered aged Al alloys. Therefore, the aim of this work is to evaluate the effect of the grinding time and grinding bodies/chips volume ratio on the properties of the metallic powder, and on the hardness of sintered samples. Considering that grinding metals requires a high ratio of grinding bodies/chips volume, 6:1, 8:1, 10:1 and 12:1 ratios were used. Grinding times of 45, 69 and 94 h were applied, in order to analyze the influence of both factors on the grinding process and, subsequently, on the mechanical properties of the obtained pieces.

2. Methodology

Al-Si-Zn-Mg alloy (supplied by a Colombian market called “Mundial de Aluminios”) chips were collected from a milling process and washed with water and detergent to remove the refrigerant. The chips were then dried and ground in a hermetic ball mill (US Stoneware East Palestine, OH 44413) with capacity of 5 L, using zirconia cylindrical ball media in air atmosphere. This ball mill consists of a hollow cylindrical shell rotating horizontally around its axis. The rotational speed used was 55 rpm. The amount of grinding bodies was 1 L. The grinding bodies/chips volume ratios and grinding times used are shown in Table 1. These values were chosen according to the literature [12,13] and considering the ductility of the aluminum. The resulting powders were characterized by X-ray diffraction (XRD), in a RIGAKU (Dmax2100) diffractometer using Cu Kα radiation; scanning electron microscopy (SEM) and energy dispersive spectroscopy (EDS), in a JEOL JSM-649 OLV Scanning Electron Microscope; and laser granulometry (LG), in a Hydro 2000MU (A), with water as dispersant.

Table 1 – Grinding bodies/chips volume ratio and grinding time of the chips.

Volume ratio	Grinding time (h)
6:1	69
	94
8:1	45
	69
	94
10:1	45
	69
	94
12:1	45
	69
	94

Given the importance of ductile or brittle behavior of metals in grinding processes, and the influence of dislocation density on such behavior, ρ (m of dislocation lines per $m^3 = /m^2$) of powders after grinding was calculated using the Eq.(1) [14]. Microstrain, η, crystallite size, d, and Burgers vector, b, were calculated from XRD patterns. b was calculated as $b = a/\sqrt{2}$, taking into account the FCC crystalline structure of aluminum, with a being the lattice parameter.

$$\rho = 2\sqrt{3}\,|\eta| / (d \times B) \quad (1)$$

Williamson and Hall method [15], as used by Baghdadi et al. [16] was used to calculate the changes in crystallite size (d) and the microstrains (η). Once d and η are obtained, b is still required to use Eq. (1) in Ref. [14], which depends on the value of a. Since lattice parameter changes with microstrains (from a value of 0.4094 nm), Burgers vector also changes. We used the Nelson-Riley method [17] to calculate a.

Subsequently, cylinders of 12.7 mm diameter and 6 mm height were compacted in a 50 Ton Enerpac press machine. The load used in the compaction processes was 19,000 lbf (equivalent to 96,800 psi), for a period of 30 s. Once the green samples were ready, they all were sintered in an oven in Ar atmosphere at 620 °C. These compaction and sintering parameters were found to be successful in a previous study [11]. The sintered samples were characterized by evaluating the relative density and Rockwell F hardness at room temperature. Additionally, Rockwell F (RF) hardness of the Al-Si-Zn-Mg bulk alloy from which the chips were obtained was measured, in

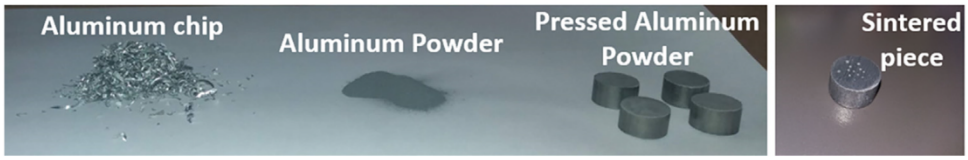

Fig. 1 – Transition from chips to sintered pieces (sintered pieces are showing indentations on its surface).

Table 2 – Chemical composition of Al-Si-Zn-Mg alloy bulk by EDS.

Chemical specie	Al	Si	Zn	Mg
Quantity (% weight)	83.93	8.10	6.78	1.19

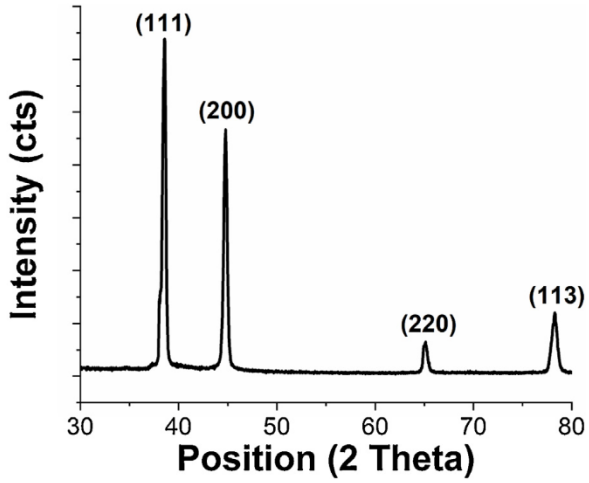

Fig. 2 – Al-Si-Zn-Mg alloy bulk XRD pattern.

order to compare it with the hardness of the pieces obtained by powder metallurgy. The relative density of the pieces was evaluated by measuring their mass, diameter and height, calculating the volume, and dividing the mass value by volume value.

According to Table 1 (from top to bottom respectively), the codification for powders and for samples obtained by compaction and sintering from the respective powders is 6:1_69 h, 6:1_94 h, 8:1_45 h, 8:1_69 h, 8:1_94 h, 10:1_45 h, 10:1_69 h, 10:1_94 h, 12:1_45 h, 12:1_69 h and 12:1_94 h.

3. Results and discussion

Fig. 1 shows the transition from chip to powder (through grinding process), to green pieces (through compaction process), and to a sintered piece (through sintering process).

3.1. *Bulk*

Al-Si-Zn-Mg alloy bulk hardness was 96.2 ± 1.0 RF. Table 2 shows the chemical species present in the alloy measured by EDS. The quantities of Si, Zn and Mg exceed the solubility in Al.

Fig. 2 depicts the XRD pattern of Al-Si-Zn-Mg alloy bulk. (111), (200), (220), and (113) peaks can be seen, which correspond to Al, according to pattern 01-085-1327. The pattern corresponds to an aged Al alloy because of the absence of peaks related to any intermetallic phase formed by Al, Si, Zn and Mg (henceforth referred to as θ), which indicates that the phase is nanometric.

Table 3 – Mean crystallite size (d) and microstrain (η) of the powders after grinding.

Grinding bodies/chips volume ratio	Grinding time (h)	d (nm)	η (%)
6:1	69	51.94	0.673
	94	48.66	0.579
8:1	45	147.3	0.464
	69	86.14	0.482
	94	88.34	0.417
10:1	45	63.33	0.581
	69	101.23	0.438
	94	142.83	0.472
12:1	45	71.12	0.531
	69	88.90	0.445
	94	48.66	0.579

3.2. *Powders after grinding*

3.2.1. *X-Ray diffraction*

Fig. 3 shows the XRD patterns of powders after grinding, varying the grinding bodies/chips volume ratio (6:1, 8:1, 10:1 and 12:1) and the grinding time (45, 69 and 94 h). The peaks corresponding to (111), (200), (220) and (113) planes can be seen, corresponding to Al, according to pattern 01-085-1327. However, other peaks also appear, corresponding to Al_2O_3 (pattern 01-071-0958). This indicates that powders are oxidizing during grinding, and the oxide formed is crystalline Al_2O_3. The absence of peaks corresponding to intermetallic phases indicates that the precipitates remain nanometric.

Table 3 shows the mean crystallite size and microstrains of the powders after grinding, according to the grinding bodies/chips volume ratio and grinding time from the Williamson-Hall method plots. Table 4 shows the lattice parameter from the *Lattice parameter* $- F(\theta)$ plots and the calculation of dislocation density.

We can see that ρ diminishes as grinding time increases from 69 h to 94 h for the 6:1 ratio. Additionally, if we observe the crystallite size in Table 3, we can see that *d* also diminishes. Plastic deformation is generated by dislocation movement during grinding. However, during dislocation movement, the dislocations themselves multiply. Taking into account that there is an increment in temperature inside the jar because of the action of the grinding bodies with the walls, and that the recrystallization of Al alloys starts around 150 °C, it is expected

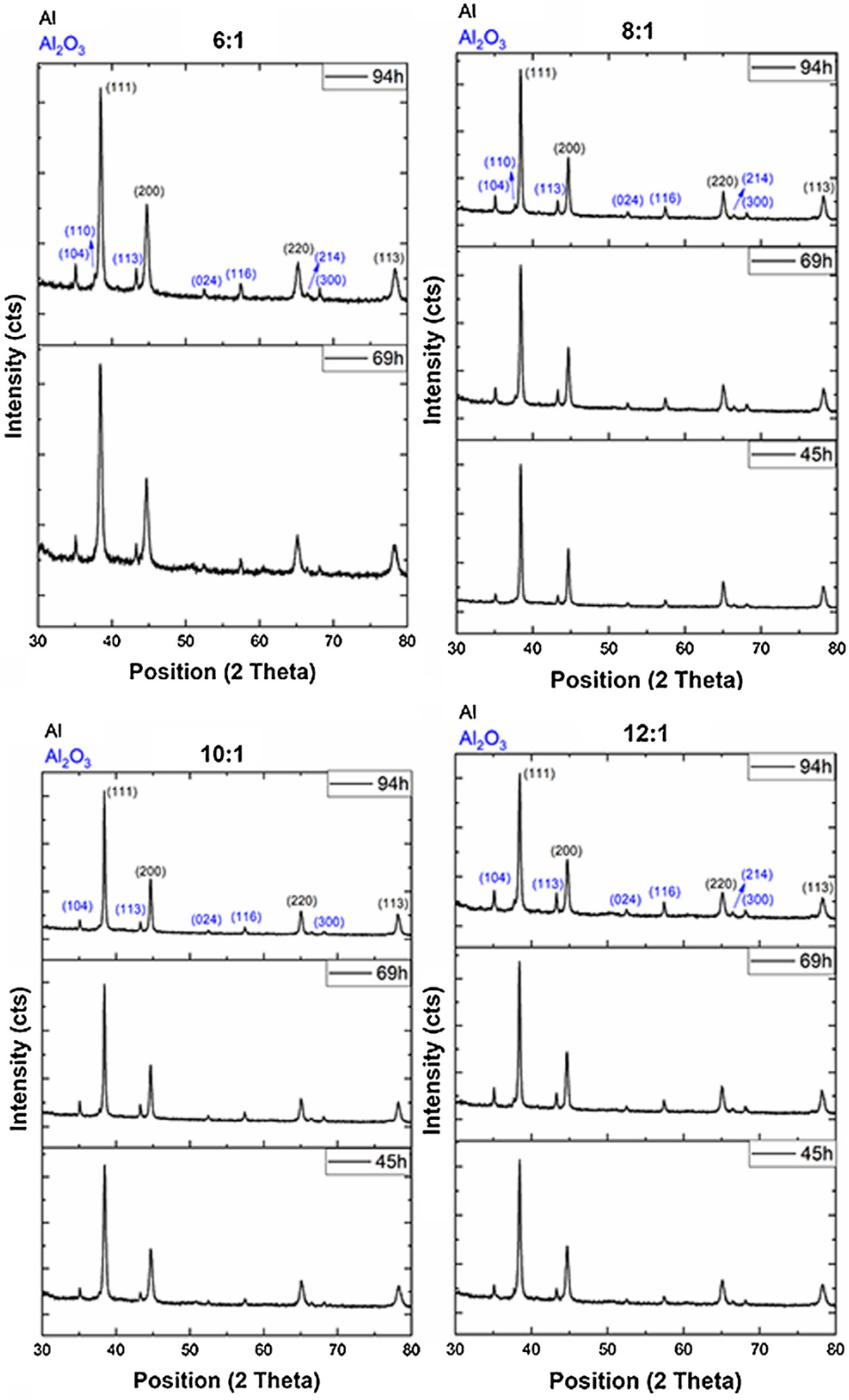

Fig. 3 – XRD pattern of the powders after grinding.

for recrystallization to occur during the process: new grain boundaries with low dislocation density are formed by the condensation dislocation walls, decreasing the system free energy [18].

Meanwhile, ρ increases as grinding time increases from 45 h to 69 h for the 8:1 ratio. This means that particles have hardened by cold working between 45 and 69 h of grinding. The multiplication of dislocations is accompanied by a

Table 4 – Calculation of dislocation density of the powders after grinding.

Grinding bodies/chips volume ratio	Grinding time (h)	Lattice parameter (nm) from Nelson-Riley method	Burgers vector, b (nm)	Dislocation density, ρ (amount/m^2)
6:1	69	0.40456	0.28607	1.5689×10^{15}
	94	0.40425	0.28585	1.4419×10^{15}
8:1	45	0.40497	0.28636	3.8150×10^{14}
	69	0.40486	0.28628	6.7706×10^{14}
	94	0.40490	0.28631	5.7115×10^{14}
10:1	45	0.40461	0.28610	1.1108×10^{15}
	69	0.40485	0.28627	5.2355×10^{14}
	94	0.40499	0.28637	3.9974×10^{14}
12:1	45	0.40469	0.28616	9.0379×10^{14}
	69	0.40485	0.28627	6.0569×10^{14}
	94	0.40468	0.28615	8.8500×10^{14}

decrease in crystallite size. The crystallite size depends on how long it has been since the last recrystallization process. This could indicate that no grain growth is completed because of the hardening and start of the next recrystallization, i.e., multiplication of dislocation occurs faster (small grains favor recrystallization processes). When grinding time increases to 94 h, dislocation density diminishes, which indicates that recrystallization has occurred.

Dislocation density diminishes as grinding time increases from 45 h to 94 h for 10:1 ratio. This means dynamic recrystallization has occurred, leading to a decrease in dislocation density. For 12:1, dislocation density diminishes as grinding time increases from 45 h to 69 h. It then increases as grinding time increases from 69 h to 94 h of grinding. This means that, at 69 h, the Al-Si-Zn-Mg alloy powder has recrystallized, and at 94 h the particles have hardened by dislocation multiplication.

Here, we can observe that time taken for critical dislocation density for dynamic recrystallization to be reached is affected by the grinding bodies/chips volume ratio of the Al-Si-Zn-Mg alloy chips grinding process. This is because the temperature inside the jar of the ball mill depends on the degree to which the grinding stock is filled. According to Schmidt et al. [19], the highest temperature is achieved without any grinding stock inside the jar. However, by adding a small amount of material to be ground, the temperature decreases considerably. This is because the added material influences the elasticity of the collisions, reducing the speed of the grinding bodies, resulting in the reduction of energy, which is dissipated as heat.

Therefore, the highest temperature reached is expected to be with the 12:1 ratio. Moreover, where there are more grinding bodies relative to the material to be ground, there are more impacts and thus more plastic deformation to the material. Thus, the higher the grinding bodies/chips volume ratio, the faster the plastic deformation—multiplication density and the recrystallization. The material ground at this ratio recrystallizes faster, while samples ground at a 6:1 ratio recrystallize more slowly. This explains the higher resultant dislocation density in the 6:1 samples than in the 12:1 samples. Therefore, in addition to heat dissipation, the quantity of material to be ground causes a damping effect. The greater the quantity of the material, the higher the effect.

There are two competing phenomena related to the grinding bodies/chips volume ratio: the higher the ratio, the higher the temperature, but the lower the damping effect.

3.2.2. *Size and morphology of particles*

Table 5 shows the powders' properties, mean particle diameter and size distribution after grinding for each grinding bodies/chips volume ratio, as a function of grinding time. The size distribution was calculated by subtracting *d(0.9)* and *d(0.1)*. It was taken into account that *d(0,1)* and *d(0,9)* are the particle sizes below which 10% and 90% respectively remain of each sample. The process of grinding brittle materials is different to that of grinding ductile materials. Brittle materials break by impact, while ductile materials suffer plastic deformation because of the movement of dislocations, which multiply during the plastic deformation, as mentioned before, before brittle fracture by impact.

With respect to the *d(0.9)-d(0.1)* value we found the tendency shown in Fig. 4a) for dislocation density, which is explained by the negative grinding phenomenon [20]. Boldyrev et al. [21] first established that, during the grinding of ceramics distortion of the crystal and dislocation appear, which influence the chemical properties of the material, resulting in mechanochemical activation. Jimbo et al. [20] subsequently found that this high surface energy also results in aggregation and agglomeration of the particles, known as the negative grinding phenomenon. This means that the higher the dislocation density, the lower the size distribution, which implies that the higher the number of dislocations, the higher the agglomeration of particles.

It is well known that high dislocation density in metallic materials implies in brittle behavior, so it is valuable to consider the dislocation density when analyzing the particle size (mean particle diameter). In this respect, the correlation shown in Fig. 4b) was found. Powders with the lowest density of dislocations, corresponding to 10:1–94 h and 8:1–45 h treatments, are those with the largest particle size. On the contrary, powders with the largest density of dislocations, corresponding to 6:1–69 h and 6:1–94 h treatments, are those with the smallest particle size. Particles with higher dislocation density behave in a more brittle manner than particles with lower dislocation density. Therefore, particles with lower dislocation density suffer more plastic deformation before breaking. Hence, it is easier to diminish the particle size when powders possess more dislocations because of their brittle-like behavior.

Also, due to the nature of metallic materials, particles can weld in cold by impact [22] during grinding. When disloca-

Table 5 – Properties of particles and sintered pieces.

Grinding bodies/ chips volume ratio	Grinding time (h)	Particles		Sintered pieces	
		Mean particle diameter (μm)	Size distribution (μm)	Apparent Density (g/cm³)	Hardness (RF)
6:1	69	37.586	58.635	2.27 ± 0.10	59.1 ± 2.65
	94	33.335	50.593	2.25 ± 0.18	68.05 ± 3.21
8:1	45	102.988	184.947	2.34 ± 0.04	62.09 ± 3.42
	69	61.758	99.395	2.33 ± 0.07	62.38 ± 2.64
	94	88.051	160.511	2.26 ± 0.04	82.43 ± 2.58
10:1	45	51.317	83.003	2.26 ± 0.06	89.37 ± 4.00
	69	64.749	111.718	2.28 ± 0.04	96.16 ± 1.84
	94	109.551	210.86	2.30 ± 0.04	70.47 ± 2.85
12:1	45	58.346	96.389	2.31 ± 0.07	62.35 ± 3.40
	69	77.243	134.601	2.50 ± 0.04	64.93 ± 2.10
	94	54.451	89.739	2.26 ± 0.06	67.58 ± 5.65

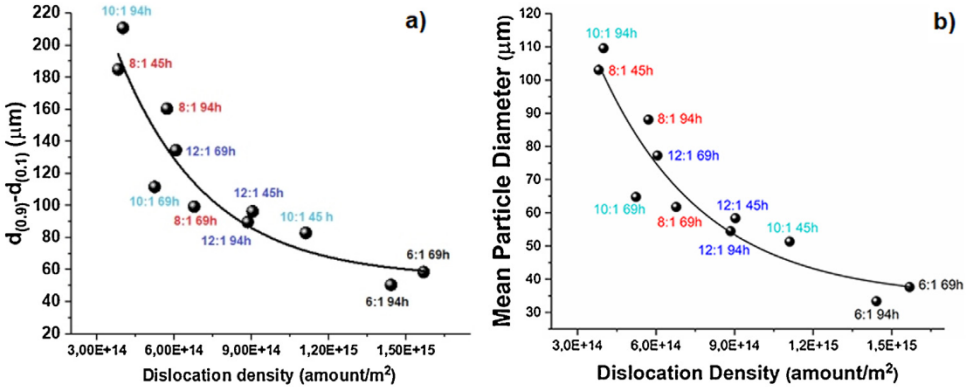

Fig. 4 – a) size distribution vs. dislocaton density and, b) mean particle diameter vs. dislocation density of the powders.

tion density is low, cold impact welding may predominate over brittle failure of particles and vice versa. This phenomenon causes particle mean diameter to increase with grinding time, as occurred in samples ground with 8:1, 10:1 and 12:1 ratios.

Fig. 5 depicts SEM micrographs of the ground powders. Consistency between the micrographs and the particle diameter shown in Table 5 can be seen, as well as plastic deformation and micro welding in some of the particles. Fig. 6 shows closer brittle failure in some powders.

3.3. *Apparent density and hardness of sintered pieces*

Table 5 also shows the sintered pieces properties: density and hardness. It can be observed that all the pieces have ~83% of the bulk density. This is attributed to porosity in the pieces after compacting and sintering the samples to form each piece, which is a common phenomenon in powder metallurgy.

After sintering, the hardness can be explained based on the particle size and particle size distribution width. The external part of the particles will create an impediment to the dislocation movement and a wide distribution of particle sizes will generate a piece with less porosity. Therefore, in Table 5 we can correlate the hardness of sintered pieces with the average particle size and with the size distribution. Treatments for 6:1–69 h and 6:1–94 h have the smallest particle sizes, so it would be expected for them to have the greatest hardness, however they present the lowest hardness value. If we observe the *d(0.9)–d(0.1)* value in the same table, we note that they have a narrow distribution, which means there are few small particles available to fill the voids left by the larger particles. In fact, according to the density values, 6:1–69 h and 6:1–94 h sintered samples exhibited the lowest density.

The trend in Table 5 shows that samples manufactured with smaller particle sizes and narrow distributions exhibit low hardness values. However, samples manufactured with large particle sizes and wide distributions also exhibit low hardness values. Meanwhile, samples manufactured with intermediate particles with an intermediate distribution, 10:1–45 h and 10:1–69 h, have higher hardness, but not all of them.

To explain this hardness behavior, it was also considered that during sintering at 620 °C for 1 h, particles were subjected to a temperature above solvus temperature and above recrystallization temperature [23]. Therefore, the processes that occurred at this stage were not only sintering and solubilization of intermetallic phase, but also recrystallization. During this recrystallization process, the initial condition of the powders is very important, as we explain below.

Fig. 7 explains what could happen during the solubilization stage (green arrow) in sintering. At room temperature, the green samples are made of α grains with the nanometric intermetallic precipitates, θ, and Al_2O_3 in the surface of

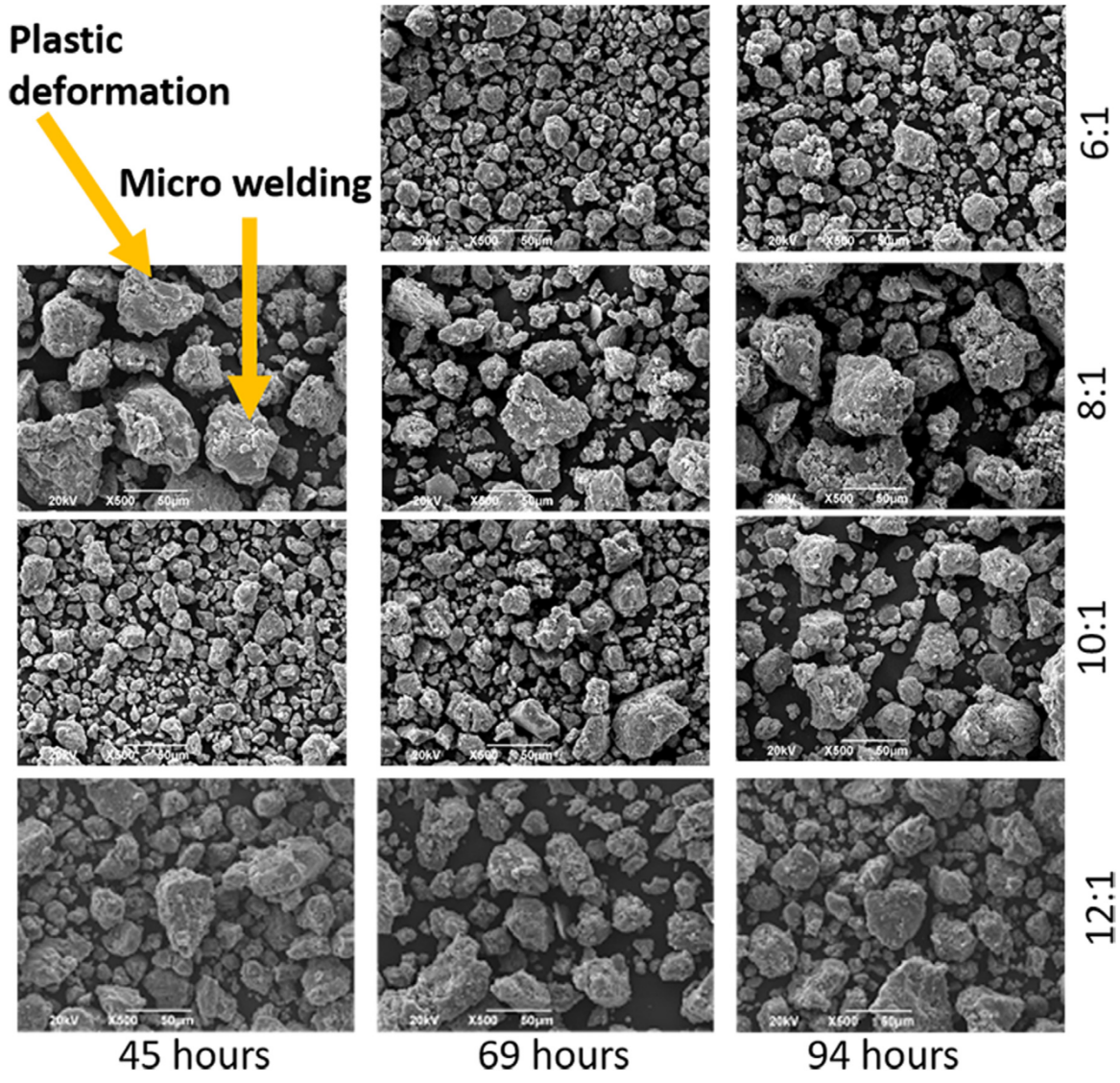

Fig. 5 – SEM images of the powders according to grinding bodies/chips volume ratio and grinding time.

the particles, according to Fig. 3. At solubilization stage, nanometric intermetallic precipitates dissolve while the sintering process is also happening. Additionally, dislocations move by diffusive processes, forming a polygonal wall inside the crystallites, because the recrystallization temperature has been exceeded. New crystallites are then formed from the polygonal wall and dislocation density diminishes, leading to a decrease in hardness. Therefore, particles with more dislocations and more area of grain boundary nucleate the new grains more quickly. Meanwhile, particles with low dislocation density and low area of grain boundary do not form new grains as quickly and, indeed, do not recrystallize during the sintering treatment if dislocation density is smaller than the critical dislocation density for recrystallization [24]. So, the relatively low dislocation density of samples 8:1–45 h, 10:1–94 h and 10:1–69 h (with a low area of grain boundary) compared with pieces at 6:1–69 h, 6:1–94 h, and 12:1–94 h (with high dislocation density and high area of grain boundary) remains, and the sintered pieces are harder.

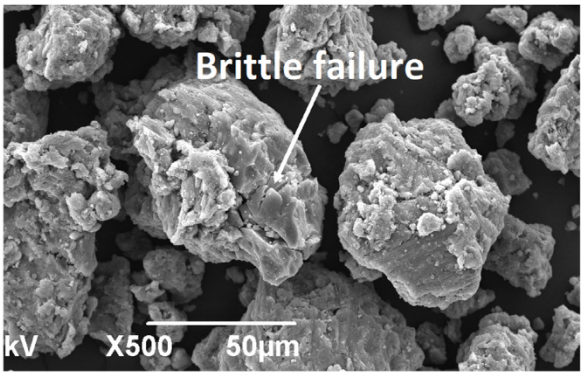

Fig. 6 – SEM image of the 8:1_45h powders.

Taking the above into account, it would be expected for the 10:1–94 and 8:1–45 h samples to present high hardness values. However, as was mentioned, these samples also exhibit a wide granulometric distribution with big particles, which

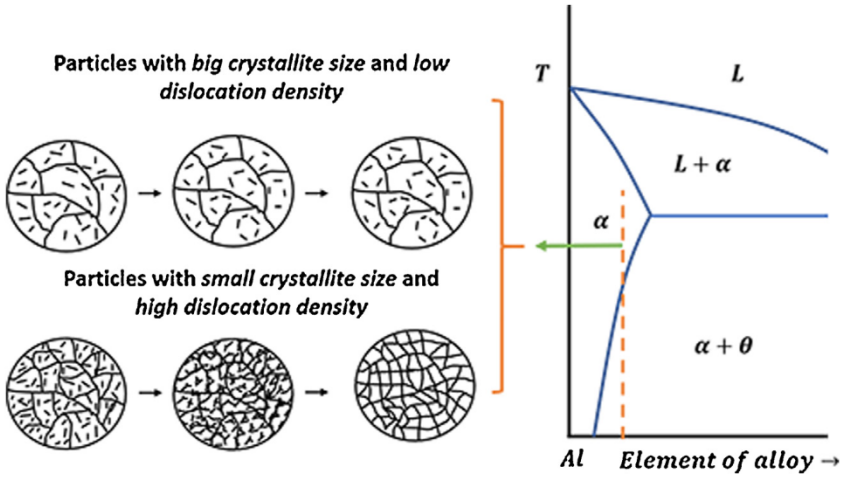

Fig. 7 – xxxx.

makes hardness low. In 10:1–45 h, a small crystallite size, an intermediate dislocation density, a low particle size, and an intermediate particle size distribution contribute to its hardness value, which is the second highest. In 8:1–94 h, a small dislocation density, the fourth treatment with the lowest dislocation density, an intermediate crystallite size, and a wide size particle distribution with relatively smaller particles contribute to it having the third highest hardness value. Finally, although 12:1–45 h, 8:1–69 h and 12:1–69 h exhibit an intermediate particle size and an intermediate distribution particle size, like 10:1–69 h, they possess higher dislocation density and lower crystallite size, which can promote recrystallization during sintering and, indeed, a decreased dislocation density, which leads to sintered pieces with low hardness.

On the other hand, it is evident that sample 10:1–69 h (96.2 ± 1.8 RF) exhibits the same hardness as the Al-Si-Zn-Mg alloy bulk (96.2 ± 2.0 RF), even though, unlike the bulk, 10:1-69 h is not aged. Therefore, the hardness of 10:1–69 h is explained by an intermediate particle size distribution, an intermediate crystallite size, a small dislocation density, and by the presence of a dispersed crystalline Al_2O_3 phase (Fig. 3), that acts as a second reinforcing phase in the sintered piece and lead to a hardness similar to the Al-Si-Zn-Mg alloy bulk.

Here one may finally remark that for analyzing and predicting the hardness of sintered pieces from metallic powders processed by powder metallurgy obtained by grinding, it is necessary to analyze not only particle size and particle size distribution, but also crystallite size and dislocation density of the particles, as these can promote (or impede) recrystallization during sintering of the pieces. Also, the reactivity of the powders with the oxygen in the environment to produce an oxide coating that could act as a second reinforcing phase is important.

4. Conclusions

Samples of metallic (Al-Si-Zn-Mg)—oxide (Al_2O_3) composite were successfully obtained through powder metallurgy technique from machining chips of a milling process. The following conclusions may be established:

- Grinding, compacting and sintering Al-Si-Zn-Mg alloy chips are associated with a way to reuse 100% of the material in order to obtain harder pieces.
- Al-Si-Zn-Mg alloy powder is formed through plastic deformation, hardening, fracture, and dynamic recrystallization during grinding.
- Dynamic recrystallization in Al-Si-Zn-Mg alloy occurs during grinding due to the increment in temperature inside the ball mill.
- Time taken for critical dislocation density for dynamic recrystallization to be reached is affected by grinding bodies/chips volume ratio in grinding Al-Si-Zn-Mg alloy chips. This ratio affects the temperature reached inside the jar and the damping effect.
- The particle size and the particle size distribution depend on the dislocation density of the powders. The higher the dislocation density the lower the size, because of the brittle behavior conferred by the high dislocation density. On the other hand, the higher the dislocation density the lower the size distribution, because of the high surface energy of the particles.
- The hardness of sintered samples obtained from metallic powders depends not only on particle size and particle granulometric distribution, but also on crystallite size and dislocation density of the particles, which could promote (or impede) recrystallization during sintering of the pieces.
- It was possible to obtain samples with lower density and higher hardness by powder metallurgy from Al-Si-Zn-Mg alloy chips than from the bulk. Powder was obtained after 69 h of grinding, using 10:1 grinding bodies/chips volume ratio, and samples were obtained by compacting at 19,000 pounds and sintering at 620 °C for 1 h. The higher hardness value was attributed to the presence of Al_2O_3 formed in the particles during grinding, which acts as a second reinforcing phase in the sintered samples, and as a retardant of intermetallic phase growing.

Conflicts of interest

The authors declare no conflicts of interest.

Acknowledgments

The authors would like to thank the research department of Escuela Colombiana de Ingeniería Julio Garavito, Colombia, for the financial support of this project.

REFERENCES

[1] Hirsch J. Recent development in aluminum for automotive applications. Trans Nonferrous Met Soc China 2014;24(7):1995–2002, http://dx.doi.org/10.1016/S1003-6326(14)63305-7.
[2] Zhang X, Chen Y, Hu J. Recent advances in the development of aerospace materials. Prog Aerosp Sci 2018;97:22–34, http://dx.doi.org/10.1016/j.paerosci.2018.01.001.
[3] Abdel-Gawad SA, Osman WM, Fekry AM. Characterization and corrosion behavior of anodized aluminum alloys for military industries applications in artificial seawater. J Surf Interfaces Mater 2019;14:314–23, http://dx.doi.org/10.1016/j.surfin.2018.08.001.
[4] Kirchener G. Der Aluminiumschrottmarkt im Wandel (in German). Aluminium 1994;70:340–3.
[5] Gronostajski JZ, Kaczmar JW, Marciniak H, Matuszak A. Direct recycling of aluminum chips into extruded products. J Mater Process Tech 1997;64:149–56, http://dx.doi.org/10.1016/S0924-0136(96)02563-0.
[6] Gronostajski J, Marcinik H, Matuszak A. New methods of aluminum and aluminum-alloy chips recycling. J Mater Process Tech 2000;106:34–9, http://dx.doi.org/10.1016/S0924-0136(00)00634-8.
[7] Irfan Ab Kadir M, Sukri Mustapa M, Abdul Latif N, Sahib Mahdi A. Microstructural analysis and mechanical properties of direct recycling aluminium chips AA6061/Al powder fabricated by uniaxial cold compaction technique. Procedia Eng 2017;184:687–94, http://dx.doi.org/10.1016/j.proeng.2017.04.141.
[8] Kumar S, Mathieux F, Onwubolu G, Chandra V. A novel powder metallurgy-based method for the recycling of aluminum adapted to a small island developing state in the Pacific. Int J Environ Conscious Des Manuf 2007;13(3,4):1–22. ECM Press.
[9] Seong-Hyeon H, Dong-Won L, Byoung-Kee K. Manufacturing of aluminum flake powder from foil scrap by dry ball milling process. J Mater Process Tech 2000;100:105–9, http://dx.doi.org/10.1016/S0924-0136(99)00469-0.
[10] Fuziana YF, Warikh ARM, Lajis MA, Azam MA, Muhammad NS. Recycling aluminium (Al 6061) chip through powder metallurgy route. Mater Res Innov 2014;18(S6):354–8, http://dx.doi.org/10.1179/1432891714Z.000000000981.
[11] Rojas-Díaz LM, Verano-Jiménez LE, Muñoz-García E, Esguerra-Arce J, Esguerra-Arce A. Production and characterization of aluminum powder derived from mechanical saw chips and its processing through powder metallurgy. Powder Technol 2020;360:301–11, http://dx.doi.org/10.1016/j.powtec.2019.10.028.
[12] Afshari Elham, Ghambari Mohammad. Characterization of pre-alloyed tin bronze powder prepared by recycling machining chips using jet milling. Mater Des 2016;103:201–8, http://dx.doi.org/10.1016/j.matdes.2016.04.064.
[13] Zhou Haiping, Hu Lianxi, Sun Yu, Zhang Hongbin, Duan Congwen, Yu Huan. Synthesis of nanocrystalline AZ31 magnesium alloy with titanium addition by mechanical milling. Mater Charact 2016;113:108–16, http://dx.doi.org/10.1016/j.matchar.2016.01.014.
[14] Susila P, Sturm D, Heilmaier M, Murty BS, Subramanya Sarma V. Microstructural studies on nanocrystalline oxide dispersion strengthened austenitic ($Fe–18Cr–8Ni–2W–0.25Y_2O_3$) alloy synthesized by high energy ball milling and vacuum hot pressing. J Mater Sci 2010;45(17):4858–67, http://dx.doi.org/10.1007/s10853-010-4264-3.
[15] Williamson GK, Hall WH. X-ray line broadening from filed aluminium and wolfram. Acta Metall Mater 1953;1:22–31, http://dx.doi.org/10.1016/0001-6160(53)90006-6.
[16] Baghdadi A, Rajabi A, Mohamad Selamat NF, Sajuri Z, Zaidi Omar M. Effect of post-weld heat treatment on mechanical behaviour and dislocation density of friction stir welded Al6061. Mat Sci Eng A 2019;754:728–34, http://dx.doi.org/10.1016/j.msea.2019.03.017.
[17] Tsai DS, Chin TS, Hsu SE, Hung MP. A simple method for the determination of lattice parameters from powder X-ray diffraction data. Mater T JIM 1989;30:474–9, http://dx.doi.org/10.2320/matertrans1989.30.474.
[18] Bacca M, Hayhurst DR, McMeeking RM. Continuous dynamic recrystallization during severe plastic deformation. Mech Mater 2015;90:148–56, http://dx.doi.org/10.1016/j.mechmat.2015.05.008.
[19] Schmidt R, Mastin Scholze H, Stolle A. Temperature progression in a mixer ball mill. Int J Ind Chem 2016;7:181–6, http://dx.doi.org/10.1007/s40090-016-0078-8.
[20] Jimbo G, Zhao QQ, Yokoyana T, Taniyana Y. The grinding limit and the negative grinding phenomenon. In: Proc. IInd World Congress of Particle Technology. Society of Powder Technology. 1990. p. 305–12.
[21] Boldyrev VV, Pavlov SV, Goldberg EL. Interrelation between fine grinding and mechanical activation. Int J Miner Process 1996;44–45:181–5.
[22] Kapila A, Lee T, Vivek A, Cooper R, Hetrick E, Daehn G. Spot impact welding of an age-hardening aluminum alloy: process, structure and properties. J Manuf Processes 2019;37:42–5, http://dx.doi.org/10.1016/j.jmapro.2018.11.006.
[23] Zhang JX, Sun HY, Li J, Liu WC. Effect of precipitation state on recrystallization texture of continuous cast AA 2037 aluminum alloy. Mater Sci Eng A 2019;754:491–501, http://dx.doi.org/10.1016/j.msea.2019.03.107.
[24] Zhang T, Shi-hong L, Yun-xin W, Gong H. Optimization of deformation parameters of dynamic recrystallization for 7055 aluminum alloy by cellular automaton. Trans Nonferrous Met Soc China 2017;27:1327–37, http://dx.doi.org/10.1016/S1003-6326(17)60154-7.